Nanoscale

Accepted Manuscript

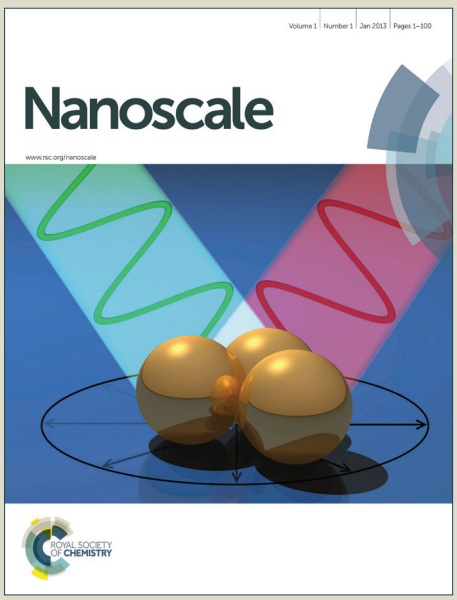

ROYAL SOCIETY OF CHEMISTRY

www.rsc.org/nanoscale

Journal Name

RSCPublishing

ARTICLE

Short-Range Ordered-Disordered Transition of NiOOH/Ni(OH)$_2$ Pair Induces Switchable Wettability

Cite this: DOI: 10.1039/x0xx00000x

Ya-Huei Chang, [a] Nga Yu Hau,[a] Chang Liu,[a] Yu-Ting Huang,[a] Chien-Cheng Li,[a] Kaimin Shih,[b] Shien-Ping Feng*, [a]

Received 00th January 2012,
Accepted 00th January 2012

DOI: 10.1039/x0xx00000x

www.rsc.org/

By virtue of amorphous structure with short-range order feature, the inorganic nanoporous nickel oxyhydroxide (NiOOH) can reversibly and rapidly switch wettability by alternate treatments of environmental chamber (superhydrophobic) and UV/ozone (superhydrophilic). The switchable mechanism of NiOOH/Ni(OH)$_2$ pair arising from its exceptional intrinsic short-range order-disorder transition together with chemical composition change is highlighted for the first time, which significantly differs from the current stimuli-responsive materials. This distinct multifunctional thin film not only owns reversible wettability but also is optically patternable/repairable and electrically conductive, which would be applicable in the manufacturing of various micro- and nanostructures. We demonstrate this potential in the rewritable two-dimensional (2D) microfluidic channels and wetting-contrast enhanced selective electroplating.

Introduction

The ability of plants to adapt to various habitats includes a range of unique wetting properties such as low-adhesivity/superhydrophobicity in the lotus leaf and high-adhesivity/superhydrophobicity in the peanut leaf.[1] Human-engineered analogues of superhydrophobic surfaces are commonly synthesized from hierarchies permanently modified with low surface energy materials so that they only allow one-way wetting transitions.[2] Recently, stimuli-responsive materials which are dynamically adaptive to the external environment, with reversibly switchable and rewritable wettability, have become attractive for various applications, including micro-patterning, cell encapsulation, microfluidic channels, and drug delivery.[3, 4] A variety of organic and inorganic materials based on the responsive mechanisms of single stimulus or multi-stimuli have been developed.[2, 5, 6] However, the sharp trade-off between the response time and the wettability switching range limits their widespread use. Most organic materials, such as photosensitive azobenzene, thermal-responsive poly(N-isopropylacrylamide)(PNIAAm), and solvent-responsive block copolymer composed of polystyrene and poly(acrylic acid), offer rapid responses (of several minutes) to versatile stimuli but show small changes (<40°) in their water contact angles (WCAs) due to their inherently smooth surfaces.[7-10] To widen the switching range, additional fabrication processes or polymer nanocomposite are usually implanted to roughen the surface, which increases process complexity. In contrast, inorganic materials have intrinsically superior switching ranges (>70°) and readily form the micro-/nano-/hierarchical structures required to reach a widely switchable wettability.[11-13] For example, two photosensitive inorganic materials, aligned nanorod ZnO film and lotus leaf-like TiO_2, enable the switching range between superhydrophobic and superhydrophilic.[14-16] Compared to organic materials, inorganic materials usually have lower toxicity and greater photochemical/thermal stability. Nevertheless, the relative long response time (several days or weeks) upon dark storage poses a significant hurdle for their practical application.[12] It is thus imperative to develop a new stimuli-responsive material that has both rapidly responsive synergic features and wide switching ranges between superhydrophilic and superhydrophobic. More importantly, if such a stimuli-responsive material could be easily patternized with readily available trigger sources, it would be viable for use in industry.

As an earth-abundant semiconductor, nickel oxyhydroxide/nickel hydroxide (NiOOH/Ni(OH)$_2$) is used in a diverse range of highly technological applications.[17-19] Nearly all of its applications are focused on its optical, electrochromic, and electrochemical properties. In previous study, we have demonstrated its great promise in terms of tunable wettability, changing from superhydrophilic to superhydrophobic via the

chemical modification of low surface-energy ODS-SAMs. However, the irreversible one-way nature of the wetting transition limits its flexibility too much for use in many cutting-edge applications.[20] In this paper, we further explore the switchable wettability of amorphous and nanoporous (AN) NiOOH/$Ni(OH)_2$. Aria and Gharib applied ultraviolet (UV)/ozone and vacuum pyrolysis treatments to the carbon nanotube to reversibly tune the wettability between hydrophilic and superhydrophobic due to the oxygen adsorption and desorption.[21] Similarly, without the need for surface chemical modification, alternately exposing the AN NiOOH/$Ni(OH)_2$ to an environmental chamber (EC, at 85°C, 70% relative humidity and normal pressure) and UV/ozone enables a rapid, reversible and widely switchable wettability between (super)hydrophobic and superhydrophilic. Interestingly, the mechanism is based on its exceptional intrinsic short-range order-disorder transition together with chemical composition change, which is highlighted for the first time. Furthermore, we found that this electrically conductive film is easily patternable and repairable, both of which are essential properties for use in smart microelectronic devices. The effectiveness of these functions was demonstrated through rewritable two-dimensional (2D) microfluidic channels and wetting-contrast enhanced selective electroplating.

EXPERIMENTAL SECTION

Fabrication of wettability-switchable film. The experiments were carried out using an anodically electroplated NiOOH/$Ni(OH)_2$ film on flat FTO glass (Rrms: 30.4 nm) and rough SS (Rrms: 110.4 nm). The electrolyte was composed of 0.39 M nickel sulfate, 0.1 M sodium sulfate, and 0.13 M sodium acetate, which was the carbonyl source indicated in the XPS. An electrochemical workstation (CHI 660E) was applied in a standard three-electrode system with the clean FTO or SS as the working electrodes, a platinum mesh as the counter electrode, and a saturated Ag/AgCl as the reference electrode. A three-step constant current densities deposition was used, starting from a current density of 0.005 mA/cm^2, then jumping to 0.05 mA/cm^2 and continuingly jump to 0.5 mA/cm^2 for every 30 mins at room temperature (see Fig S1, Supporting Information). The reasons for using three-step anodic electrodeposition are explained in our previous work[20]. The deposited film exhibited the same electrical conductivity (7.6 Ω/□) as the bare substrates even after exposure to EC at 50°C and 85°C with 70% RH (HongHui, THH80L) or a hot plate at 100°C for 60 mins and UV/ozone (Kingo, TK-110) for 10 mins.

Optical patterning process. As shown in Fig. 1(a), a UV/ozone-resist sticker was ablated with a CO_2 laser (Universal Laser System) to arbitrarily generate the desired mask in the microscale, including the Y-shaped and the 'smiling face' pattern for the rewritable 2D microfluidic channels, and the vertical strips for the wetting-contrast enhanced selective plating. Second, the patterned mask was attached to the $Ni(OH)_2$-coated FTO surface (WCAs ~ 139°) and then exposed to UV/ozone (WCAs of exposed area < 4°). Last, after the sticker was removed, a superhydrophilic-hydrophobic pattern was produced in two applications. Before rewriting a new pattern, ethanol was used to clean off the sticker residue. Fig. 1(e) is a schematic of Y-shaped 2D microfluidic channels. The commercial gold (Samtec) and nickel (Caswell) electrolytes were used for electroplating for 270s.

Characterization. WCAs were measured by a contact angle goniometer (Sindatek Model 100SB) at five points. The film atomic structure, morphology, crystallinity, and chemical state were determined by HRTEM (Tecnai, G220S-Twin), FE-SEM (Hitachi S-4800), grazing-angle XRD (Rigaku Smatlab) with an incident angle of 0.15°, and XPS (Physical Electronics 5600).

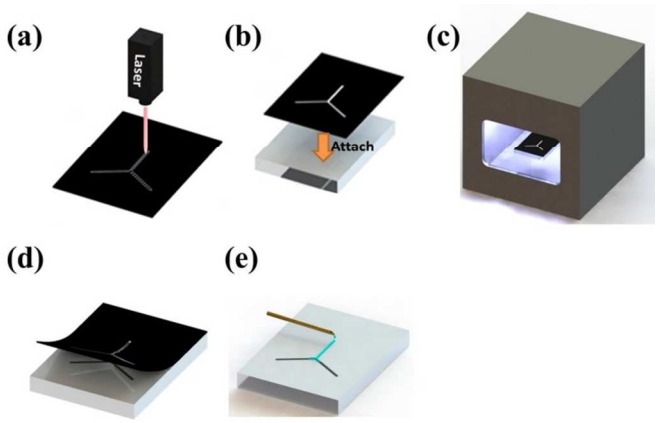

Fig. 1. The representative process flow for patterning. (a) A UV/ozone resisted sticker was ablated to a hollow Y shaped sticker with a CO_2 laser. (b) The patterned sticker was attached to $Ni(OH)_2$-coated FTO glass. (c) The exposed Y-shaped $Ni(OH)_2$ film reacted with UV/ozone. (d) The sticker was removed and a gray Y-shaped NiOOH channel was formed. (e) The microfluidic drops flowed along the superhydrophilic NiOOH film surrounded by hydrophobic $Ni(OH)_2$ film.

RESULTS AND DISCUSSION

AN NiOOH with a thickness of 600 nm was deposited on flat fluorine-doped tin oxide (FTO) glass (see Fig. 2(a) and (b)) and rough stainless steel (SS) via stepwise anodic electrodeposition, which is cost-effective and relatively fast, and in which it is easy to control and reproduce surface morphologies.[22] Fig. 2(c) shows the reversible wettability of the AN NiOOH/$Ni(OH)_2$-coated substrates. The as-prepared nanoporous film on FTO was dark and superhydrophilic (6.9±1°). After being heated on a hot plate (100°C), the film became transparent and hydrophobic (112.5±5°). This change in coloration implied a change of chemical composition within the film.[23] The EC (85°C, 70% RH) was introduced to the heat treatment with sufficient water vapor. The WCAs increased to 138.9±3° after exposure to the EC, indicating that water vapor plays an important role in mediating wettability. When the surface was irradiated with UV/ozone (265 nm), the color and WCAs were restored to their initial states. The film not only owns the long-term stability stored at ambient atmosphere but also good reversibility over than 10 cycles (Fig. S2). Using the rough SS (Fig. S3,) instead of the flat FTO as a substrate further broadened the switchable wettability ranges from superhydrophilic (4.1±1°) to superhydrophobic (153.2±2°) due to the improved 3D capillary effect and air-trapping effect.[24, 25] The excellent water-repellency (see video S2) on AN NiOOH/$Ni(OH)_2$-coated SS was achieved. The adhesion force between water droplet and sample was calculated to be around 33 μN (see Fig. S4).[26]

Conventional x-ray diffraction (XRD), as shown in Fig. S5, revealed amorphous features in the films coated on FTO under different treatment conditions. Further atomic-scale information was acquired from high-resolution transmission electron microscopy (HRTEM).

As shown in Fig. 3(a), the as-prepared film was short-range ordered γ-NiOOH with a basal spacing of 6.7 Å, in which the atomic packing of layered nanosheets was in the [00l] direction

with intercalated water molecules and alkali metal ions.[27] The intersheet distance was found to be slightly shorter than the theoretical value (6.9 Å), which may be attributed to the lattice distortion.[28] Because the sponge-like nanoporous structure can enhance the 3D capillary effect and the edge plane of γ-NiOOH has a high affinity toward water, the combined effect results in superhydrophilicity.[24] When subject to the EC of 50°C and 70% RH (shortened to low EC, hereafter), trivalent γ-NiOOH was reduced to short-range ordered α-$Ni(OH)_2$ with an expanded basal spacing of 7.6 Å, and WCAs were increased to near 90° due to the hydrophobic basal plane of $Ni(OH)_2$, as shown in Fig. 3(b).[29] According to equation (1), the chemical reaction induces the composition change from NiOOH to $Ni(OH)_2$ when consistently supplied with water vapor.[23]

$$NiOOH + H_2O + e^- \rightarrow Ni(OH)_2 + OH^- \quad (1)$$

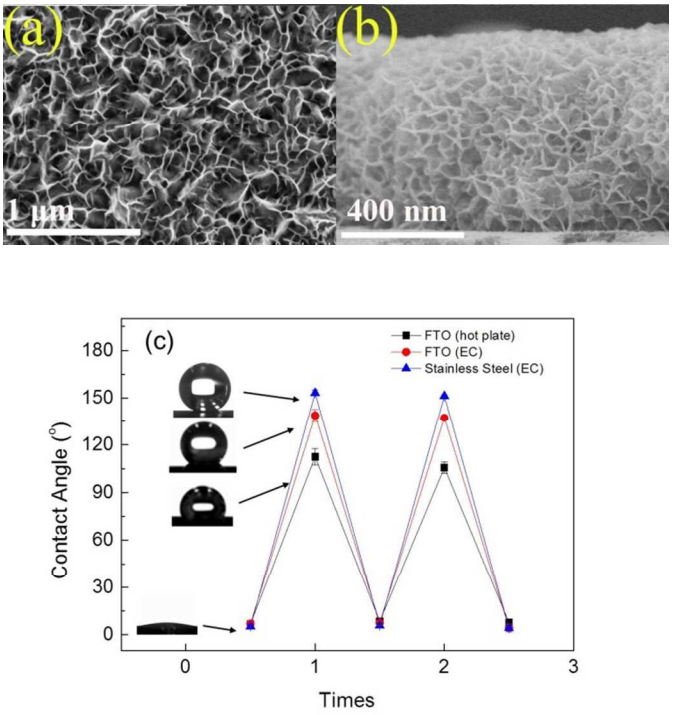

Fig. 2. FE-SEM images of as-prepared film from (a) top and (b) side view. (c) Reversible change in wettability of as-prepared film and its alternate exposure to different heat sources and UV/ozone on FTO and SS.

The α-$Ni(OH)_2$ belongs to simple layered double hydroxide (Ni-LDH), which is constructed from a stacked $Ni(OH)_{2-x}$ layer (symmetry: D_{3h} or O_h) intercalated with anions and water molecules (C_{2v}) in between. As noted, the unmatched symmetry between water molecules and $Ni(OH)_{2-x}$ layers inevitably causes defects due to turbostratic disorder (α-$Ni(OH)_2$) but maintains a short-range order along the [00l] direction.[30]

As shown in Fig. 3(c), heating at relatively high temperatures of 85°C and 70% RH (shortened to high EC, hereafter) caused not only the chemical composition to change but also an order-disorder transition of $Ni(OH)_2$, where the edge plane was ill-defined and the layered structure completely disappeared. This could be explained by the local rearrangement of crystallographic orientation to optimize the hydrogen bonding between the thermal-diffused/intercalated water and the $Ni(OH)_{2-x}$ layer.[31, 32] From thermodynamic point of view, the short-range ordered $Ni(OH)_2$ layers tilt a certain angle to enable their lowest surface-energy (00ℓ) planes to face the air (see Fig. S6), leading to a nanoscale discontinuous three-phase contact line (TCL).[1] As a result, the presence of disordered structures tends towards air traps rather than water adsorption to further increase WCAs. Fig. 4 illustrates the mechanism of de-wetting evolution from as-prepared to high EC treated samples, where the hydrophobic regions are extended from basal plane (low EC) to edge plane (high EC) of $Ni(OH)_2$ after the EC treatment. Taking advantage of the mild oxidation and hydrolyzation caused by UV/ozone to provide hydroxyl radicals, the film was returned to a superhydrophilic γ-NiOOH phase, as shown in Fig. 3(d).[33]

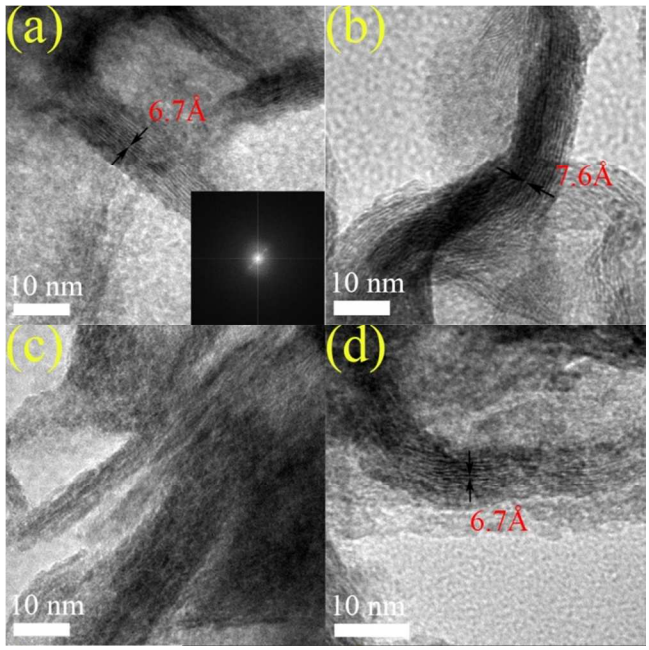

Fig. 3. HR-TEM images of (a) as-prepared film and its exposure to (b) low EC, (c) high EC for 1 hr, and (d) UV/ozone for 10 min.

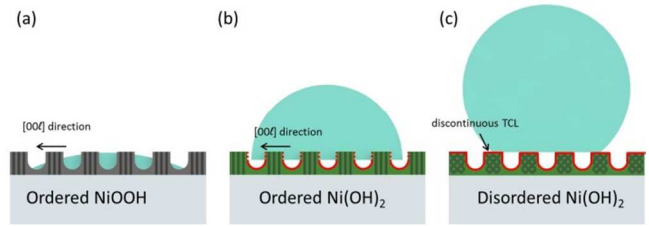

Fig. 4. The mechanism of de-wetting evolution of an (a) as-prepared sample, (b) low EC treated sample and (c) high EC treated sample. Hydrophobic regions in (b) and (c) are marked with red curves.

To mitigate undesired substrate signals, grazing incidence XRD was used to evaluate the global film evolution arising from the chemical composition change and the short-range order-disorder transition as shown in Fig. 5.[34] The peak positions of amorphous hump were located at 13.2° for as-prepared and UV/ozone samples, corresponding to the prominent basal reflection (001) of crystallized γ-NiOOH, and the peak at 11.6° for low EC treated sample corresponded to α-$Ni(OH)_2$. The relatively low intensity of high EC treated film provides evidence for the disordered characteristics outlined previously.[35]

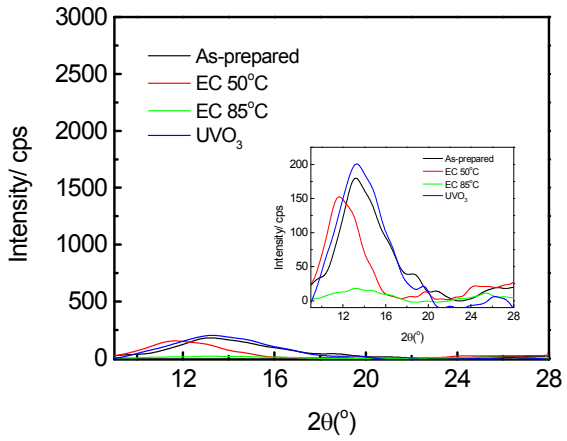

Fig. 5. Grazing incidence XRD of as-prepared film and its exposure to low EC, high EC for 1 hr, and UV/ozone for 10 mins. The inset shows its enlargement.

X-ray photoelectron spectroscopy (XPS) provided not only the surface chemical state but also the surface water adsorption, enabling us to construct a comprehensive picture of the film's surface status, as seen in Fig. 6. In the Ni 2p region, as-prepared and UV/ozone treated samples exhibit identical spectra with two peaks centered at 856.6 eV and 873.9 eV, corresponding to Ni $2p_{3/2}$ and Ni $2p_{1/2}$ for γ-NiOOH. The high EC treated sample, however, shifts to lower binding energy at 855.2 eV and 872.9 eV corresponding to Ni $2p_{3/2}$ and Ni $2p_{1/2}$ for $Ni(OH)_2$.[36] O 1s spectra of as-prepared and UV/ozone-treated samples were deconvoluted into four peaks assigned respectively to lattice O^{2-} (529.5 eV), OH^- (531.1 eV), carbonyl groups (531.7 eV) and hydroscopic H_2O (532.2 eV), whereas the high EC treated sample was only composed of OH^- (531.1 eV) and carbonyl groups (531.7 eV).[37] Table S1 shows that the normalized O^{2-}/OH^- ratios for as-prepared, high EC treated and UV/ozone-treated samples were 0.97, 0 and 0.32 respectively, indicating that as-prepared stoichiometric γ-NiOOH was converted to surface water-deficient $Ni(OH)_2$ via EC treatment, and then transformed into OH^--enriched γ-NiOOH after UV/ozone irradiation. The amounts of hydroscopic H_2O can be taken as a good index of surface affinity towards water, which are in good agreement with the wetting behavior of the as-prepared and UV/ozone treated samples and the de-wetting behavior of the EC treated sample. As noted, the relatively strong hydroscopic water peak of the UV/ozone treated sample is believed to result from the high amount of hydroxyl radicals generated during the UV/ozone process. The resulting OH^--enriched γ-NiOOH can enhance water adsorption, leading to low WCAs.

To advance our understanding of the kinetic mechanism, the time dependence of WCAs upon EC treatment at 85°C and 120°C was monitored, as shown in Fig. 7.

The experimental data was fitted by the dynamic Cassie model. We assume that the composite film surface purely consists of NiOOH and $Ni(OH)_2$, and their kinetic decline/growth follows Avrami's law as expressed in equation 2.[38, 39]

$$\cos\theta = \cos\theta_{NiOOH}\, a\exp(-kt^n) + \cos\theta_{Ni(OH)_2}\,[1 - a\exp(-kt^n)] \quad (2)$$

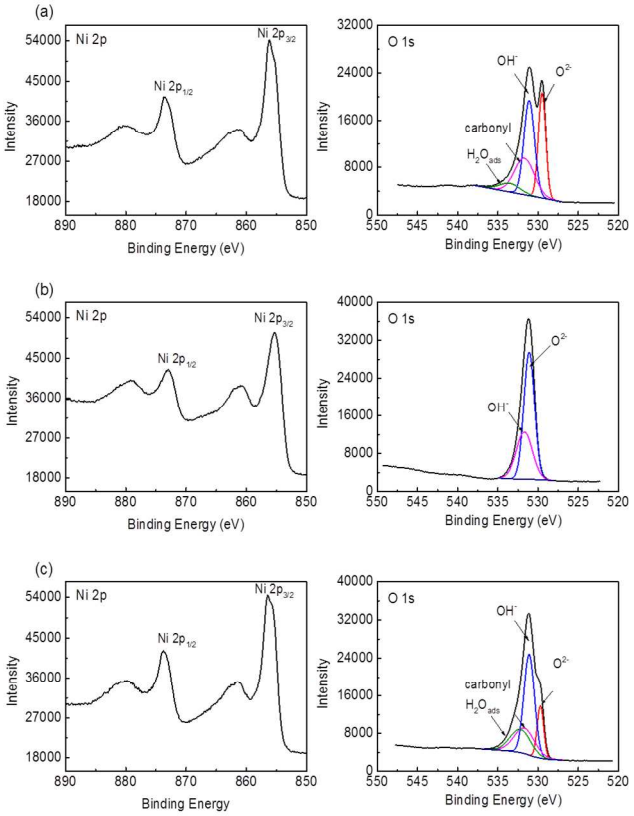

Figure 6. XPS of (a) as-prepared film and its exposure to (b) high EC for 1 hr, and (c) UV/ozone for 10 mins

where θ_{NiOOH} and $\theta_{Ni(OH)_2}$ are WCAs for ordered NiOOH and disordered $Ni(OH)_2$, respectively, a is the initial surface coverage of ordered NiOOH, k is the Avrami constant, and n is the Avrami exponent. Two theoretical boundary conditions at t=0 and t=∞ represent the pure ordered NiOOH and pure disordered $Ni(OH)_2$ constitutions respectively. The fitting exponent n is 1.55, which belongs to 2D nucleation/growth. The initial ordered NiOOH coverage is 100% (a=1), which is consistent with the XPS results. According to k values of a rate constant at two different temperatures, Arrhenius activation energy is 18.48 kJ/K·mole. This value is in the same scale of reported activation energy for electrical reduction from NiOOH to $Ni(OH)_2$.[35] Here we summarize a model that explains this de-wetting evolution, including sequential reactions induced by thermal energy and water vapor: (i) short range ordered γ-NiOOH converts to short-range ordered α-$Ni(OH)_2$ and (ii) defect-driven crystallographic rearrangement between thermal-diffused/intercalated water and $Ni(OH)_{2-x}$ layer to form disordered $Ni(OH)_2$.

As mentioned above, AN NiOOH/$Ni(OH)_2$ film has achieved a rapid response for switchable wettability between superhydrophilic and (super)hydrophobic without changing its surface morphologies. These outperforming features could be used in a wide variety of applications. We demonstrate two such potential uses: rewritable two-dimensional (2D) microfluidic channels and wetting-contrast enhanced selective electroplating on FTO substrates. The representative patterning process is depicted in Fig. 1. Figs. 8(a)-(g) and video S3, a real-time recording, show the microfluidic flow along the superhydrophilic paths with a width of 264 μm observed with optical microscopy. The microfluidic drops propagated along

the superhydrophilic NiOOH domain and distributed into the branches, propelled by surface-tension confinement and capillary force.[40] In previous studies, the reported 2D microfluidic channels, which were usually patterned by photolithography or inject/stamp printing, formed a virtual wall between the hydrophobic and hydrophilic domains to restrict the overflow from the channel but differed in their physical microthickness.[41] Compared to these methods, our cost-effective patterning approach creates the "real" 2D bounded flow without a height difference to remarkably reduce the air friction, resulting in a flow speed of 0.82 mm/s using deionized (DI) water as microdrops. The high reversibility allows us to erase the Y-shaped pattern using high EC treatment and then rewrite a smiling face following the same patterning process, as shown in Fig. 8(h). Fig. S7 displays the wet eyes and mouth on the dry face, demonstrating how easily an arbitrary pattern with high wetting contrast can be reproduced.

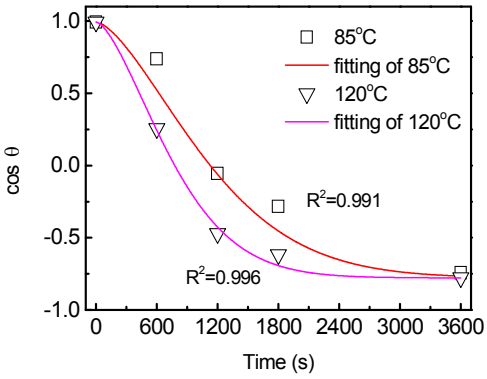

Fig. 7. Time dependence of WCAs upon EC at different temperatures.

Direct selective metal plating is of great interest for smart microelectronic devices due to the material saving and fabrication simplification. The deposition principle is to control the native differences of the substrate activities, such as doping polarity, seed cultivation, or functionalized tailored groups.[42-44] We discovered that the extreme wetting contrast is capable of opening a voltage window for selective electroplating. As shown in Fig. 9(a), gold electrodeposited on the superhydrophilic NiOOH-coated FTO surface requires a less negative onset potential (-0.94 V) than that on the hydrophobic $Ni(OH)_2$-coated FTO (-1.14 V). A similar trend can be observed in electroplated nickel, as shown in Fig. S8(a). The strip pattern was defined using the process shown in Fig. 1 and gold was then electroplated at a voltage of –1.0 V within the operation window. Fig. 9 (b) shows that only the predetermined superhydrophilic NiOOH strips were selectively electroplated. The selectively electroplated nickel can be reproduced using the same process (see inset of Fig. S8(a)). This wetting-contrast enhanced selective electroplating occurs when operating within the optimum voltage range because the superhydrophilic NiOOH surface has high surface energy, leading gold to preferentially deposit on it to reduce the total surface energy. The hydrophobic $Ni(OH)_2$ surface has a low surface energy that blocks gold deposition. Fig. S8(b) shows that gold nanoparticles only nucleate and grow on the scaffolds of hydrophobic $Ni(OH)_2$ film even at high overpotential (-2V), demonstrating the great lyophobicity of gold electrolytes.

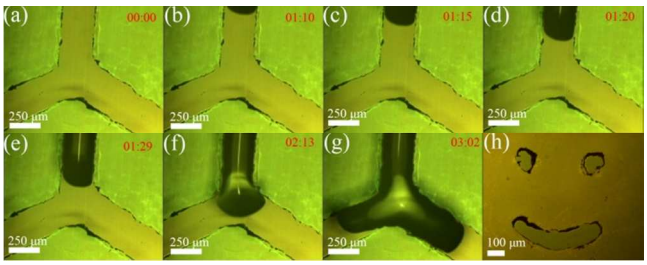

Fig. 8. (a)-(g) The OM images of the dynamic recording of the microflow in 2D microfluidic channels with a magnification of 100X within 3:02s, and (h) the rewritten superhydrophilic NiOOH smiling face pattern on hydrophobic $Ni(OH)_2$-coated FTO glass.

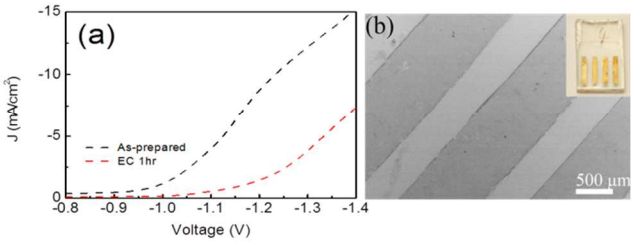

Fig. 9. (a) Cathodic waves of cyclic voltammetry for gold. (b) FE-SEM image of golden strips. The inset shows its photograph.

Conclusions

The conclusions section should come at the end of article, before the acknowledgements. In summary, we have presented a wettability switchable material of AN NiOOH/$Ni(OH)_2$ film that demonstrates synergy between response time and switching ranges. A switching cycle starting from superhydrophilic to superhydrophobic (in an EC of 85°C, 70% RH) and reversing back to superhydrophilic (upon UV/ozone irradiation) can be accomplished within 70 mins. HR-TEM and grazing incidence XRD provide evidence that the transformation of chemical composition and the transition of short-range order-disorder are responsible for the successive de-wetting behavior. The de-wetting kinetics is correlated to the 2D nucleation and growth model resulting from the serial reactions of NiOOH/$Ni(OH)_2$ conversion and the defect-driven rearrangement of crystallographic orientation. The impressive features of AN NiOOH/$Ni(OH)_2$ film, including widely switchable wettability, rapid response time, good electrical properties and ease of patternization, are expected to open up a new approach in a wide variety of applications. Here, two such potential applications, rewritable 2D microfluidic channels and the wetting-contrast enhanced selective electroplating, have been demonstrated via a cost-effective optical patterning technique.

Acknowledgements

This work was supported by the General Research Fund from Research Grants Council of Hong Kong Special Administrative Region, China, under Award Number: HKU 712213E.

Notes and references

[a] Department of Mechanical Engineering, The University of Hong Kong, Pokfulam Rd., Hong Kong. Email: hpfeng@hku.hk

[b] Department of Civil Engineering, The University of Hong Kong, Pokfulam Rd., Hong Kong.

Electronic Supplementary Information (ESI) available: [details of any supplementary information available should be included here]. DOI: 10.1039/b000000x/

1. S. Yang, J. Ju, Y. Qiu, Y. He, X. Wang, S. Dou, K. Liu and L. Jiang, *Small*, 2014, **10**, 294-299.
2. X. J. Feng and L. Jiang, *Adv. Mater.*, 2006, **18**, 3063-3078.
3. M. A. C. Stuart, W. T. S. Huck, J. Genzer, M. Muller, C. Ober, M. Stamm, G. B. Sukhorukov, I. Szleifer, V. V. Tsukruk, M. Urban, F. Winnik, S. Zauscher, I. Luzinov and S. Minko, *Nature Mater.*, 2010, **9**, 101-113.
4. E. Ueda and P. A. Levkin, *Adv. Mater.*, 2013, **25**, 1234-1247.
5. B. Xin and J. Hao, *Chem. Soc. Rev.*, 2010, **39**, 769-782.
6. J. Zhuang, M. R. Gordon, J. Ventura, L. Li and S. Thayumanavan, *Chem. Soc. Rev.*, 2013, **42**, 7421-7435.
7. N. Delorme, J. F. Bardeau, A. Bulou and F. Poncin-Epaillard, *Langmuir*, 2005, **21**, 12278-12282.
8. S. Kidoaki, S. Ohya, Y. Nakayama and T. Matsuda, *Langmuir*, 2001, **17**, 2402-2407.
9. D. Julthongpiput, Y.-H. Lin, J. Teng, E. R. Zubarev and V. V. Tsukruk, *Langmuir*, 2003, **19**, 7832-7836.
10. D. Mecerreyes, V. Alvaro, I. Cantero, M. Bengoetxea, P. A. Calvo, H. Grande, J. Rodriguez and J. A. Pomposo, *Adv. Mater.*, 2002, **14**, 749-752.
11. G. Caputo, C. Nobile, T. Kipp, L. Blasi, V. Grillo, E. Carlino, L. Manna, R. Cingolani, P. D. Cozzoli and A. Athanassiou, *J. Phys. Chem. C*, 2008, **112**, 701-714.
12. R.D. Sun, A. Nakajima, A. Fujishima, T. Watanabe and K. Hashimoto, *J. Phys. Chem. B*, 2001, **105**, 1984-1990.
13. N. Stevens, C. I. Priest, R. Sedev and J. Ralston, *Langmuir*, 2003, **19**, 3272-3275.
14. X. Feng, L. Feng, M. Jin, J. Zhai, L. Jiang and D. Zhu, *JACS*, 2003, **126**, 62-63.
15. X. Feng, J. Zhai and L. Jiang, *Angew. Chem. Int. Ed.*, 2005, **44**, 5115-5118.
16. W. Sun, S. Zhou, P. Chen and L. Peng, *Chem. Commun.*, 2008, 603-605.
17. G. Duan, W. Cai, Y. Luo and F. Sun, *Adv. Funct. Mater.*, 2007, **17**, 644-650.
18. H. Zhang, X. Yu and P. V. Braun, *Nat. Nanotechnol.*, 2011, **6**, 277–281.
19. J. Nai, S. Wang, Y. Bai and L. Guo, *Small*, 2013, **9**, 3147-3152.
20. Y. H. Chang, Y. T. Huang, M. K. Lo, C. F. Lin, C. M. Chen and S. P. Feng, *J. Mater. Chem. A*, 2014, **2**, 1985-1990.
21. A. I. Aria and M. Gharib, *Langmuir*, 2011, **27**, 9005-9011.
22. T. Darmanin, E. T. de Givenchy, S. Amigoni and F. Guittard, *Adv. Mater.*, 2013, **25**, 1378-1394.
23. Y. Ren, W. K. Chim, L. Guo, H. Tanoto, J. Pan and S. Y. Chiam, *Sol. Energy Mater. Sol. Cells*, 2013, **116**, 83-88.
24. J. Bico, U. Thiele and D. Quéré, *Colloid Surf. A-Physicochem. Eng. Asp.*, 2002, **206**, 41-46.
25. L. Liu, J. Zhao, Y. Zhang, F. Zhao and Y. Zhang, *J. Colloid Interface Sci.*, 2011, **358**, 277-283.
26. X. D. Zhao, H. M. Fan, J. Luo, J. Ding, X.Y. Liu, B.S. Zou and Y.P. Feng, *Adv. Funct. Mater.*, 2011, **21**, 184-190.
27. L. Liu, Z. Zhou and C. Peng, *Electrochim. Acta*, 2008, **54**, 434-441.
28. C. Boissiere, D. Grosso, S. Lepoutre, L. Nicole, A. B. Bruneau and C. Sanchez, *Langmuir*, 2005, **21**, 12362-12371.
29. F. J. Micale, M. Topić, C. L. Cronan, H. Leidheiser Jr and A. C. Zettlemoyer, *J. Colloid Interface Sci.*, 1976, **55**, 540-545.
30. A. V. Radha, P. V. Kamath and C. Shivakumara, *J Phys Chem B*, 2007, **111**, 3411-3418.
31. T. N. Ramesh, R. S. Jayashree and P. V. Kamath, *Clays Clay Miner.*, 2003, **51**, 570-576.
32. T. N. Ramesh, P. V. Kamath and C. Shivakumara, *J. Electrochem. Soc.*, 2005, **152**, A806-A810.
33. C. W. Kung, H. W. Chen, C. Y. Lin, R. Vittal and K. C. Ho, *J. Power Sources*, 2012, **214**, 91-99.
34. D. R. Blasini, J. Rivnay, D.-M. Smilgies, J. D. Slinker, S. Flores-Torres, H. D. Abruna and G. G. Malliaras, *Journal of Materials Chemistry*, 2007, **17**, 1458-1461.
35. P. Oliva, J. Leonardi, J. F. Laurent, C. Delmas, J. J. Braconnier, M. Figlarz, F. Fievet and A. d. Guibert, *J. Power Sources*, 1982, **8**, 229-255.
36. M. C. Biesinger, B. P. Payne, L. W. M. Lau, A. Gerson and R. S. C. Smart, *Surf. Interface Anal.*, 2009, **41**, 324-332.
37. B. P. Payne, M. C. Biesinger and N. S. McIntyre, *J. Electron. Spectrosc. Relat. Phenom.*, 2012, **185**, 159-166.
38. S. Frenznick, S. Swaminathan, M. Stratmann and M. Rohwerder, *J. Mater. Sci.*, 2010, **45**, 2106-2111.
39. S. Farris, L. Introzzi, P. Biagioni, T. Holz, A. Schiraldi and L. Piergiovanni, *Langmuir*, 2011, **27**, 7563-7574.
40. P. Lam, K. J. Wynne and G. E. Wnek, *Langmuir*, 2002, **18**, 948-951.
41. I. You, N. Yun and H. Lee, *ChemPhysChem*, 2013, **14**, 471-481.
42. C. Scheck, P. Evans, R. Schad, G. Zangari, L. Sorba, G. Biasiol and S. Heun, *Appl. Phys. Lett.*, 2005, **86**, 133108-1-133108-3.
43. H. P. Feng, T. Paudel, B. Yu, S. Chen, Z. F. Ren and G. Chen, *Adv. Mater.*, 2011, **23**, 2454-2459.
44. N. S. Pesika, F. Fan, P. C. Searson and K. J. Stebe, *JACS*, 2005, **127**, 11960-11962.

Table of Contents

The combination of short-range ordered-disordered transition and redox reaction leads to widely and rapidly switchable wettability of nickel oxyhydroxide/nickel hydroxide.